ALGORITHMS FOR MULTI-BEAM RECEIVER DATA ANALYSIS

G. Ruiz, L. Leushacke, and J. Rosebrock

FGAN - Research Institute for High Frequency Physics and Radar Techniques (FHR), Germany.
Email: guillermo@fgan.de; leushacke@fgan.de; rosebrock@fgan.de

ABSTRACT

A series of high sensitivity debris observation campaigns conducted by FGAN's TIRA L-band radar as the primary transmitter/receiver and the new multi-beam system of the Effelsberg radio telescope as secondary receiver in bi-static beam-park mode is planned in order to improve the characterization of the population of space debris in LEO. The first of these campaigns is going to take place in 2006. The current development of a 7-beam receiver at L-band for the Effelsberg radio telescope will allow a more accurately determination of the trajectory parameters and the RCS of even sub-centimeter sized objects. For this purpose new algorithms for multi-beam data analysis have to be developed. This paper presents the theoretical basics and the performance of these algorithms.

Key words: Space debris; TIRA; the Effelsberg radio telescope; Multi-beam; RCS; Maximum Likelihood estimation (MLE); CRLB.

1. INTRODUCTION

To validate and update space debris environmental models like ESA's MASTER, especially in the 1-10 cm size class, measurements have to be conducted frequently due to the highly dynamic population. Because of their all-weather and day-and-night performance, powerful ground based radars are the most suited sensors to carry out these measurement campaigns in LEO.

Since 1994 FGAN's TIRA L-band radar has successfully taken part in ten internationally coordinated 24-hours beam-park experiments, six of them covering the LEO full altitude range (300-2000 km). Careful data analysis revealed that TIRA is capable of detecting down to 2 cm sized objects at 1000 km range. Higher detection sensitivity can currently only be achieved with the help of an additional passive receiver with a very large aperture and low noise receivers. The suitability as secondary receiver of the Effelsberg radio telescope, operated by Max Planck Institute for Radio Astronomy (MPIfR), was demonstrated in COBEAM-1/96 thanks to the 100 m aperture, the cryogenic cooled receivers and close location to TIRA of the Effelsberg facility (Leushacke, 1997). COBEAM-1/96 was also a TIRA-Effelsberg bi-static beam-park experiment, but with a single beam receiver in Effelsberg. Debris objects of 9 mm size at 1000 km range were detected for the first time in Europe during COBEAM-1/96.

The low detection level of the Effelsberg radio telescope allowed a first statistical estimation of the population density in the 1-2 cm size class. Nevertheless the RCS and the trajectory parameters of those very small objects could not be estimated from the COBEAM-1/96 results due to the ambiguities caused by the antenna pattern's side lobes. The necessity for an exact knowledge of the object RCS forced to equip the Effelsberg radio telescope with a multi-beam receiver and to develop new analysis algorithms, in order to be able to resolve the ambiguities by matching the information from the different beams. For this purpose a 7-horn multi-feed at L-band for the Effelsberg radio telescope is being developed by MPIfR under ESA/ESOC contract. This multi-beam system will supply 14 independent channels, since each of the seven horns will provide two channels with orthogonal polarization. The central horn will have circular polarization and the six outer horns linear polarization. The footprint at sky of the Effelsberg multi-beam system is sketched in Fig. 1. The beam axes are represented as solid points and their 3 dB beam widths as solid circles ($Q_{3dB} \approx 0.16^o$). An object's passage example with passage offset Θ and passage direction Φ is also illustrated. Straight trajectories can be assumed due to the short passage duration.

As shown in Fig. 1 the multiple beams do not overlap. That means that monopulse techniques can be used neither for the extraction of the passage parameters, nor for determination of the object RCS like with TIRA, because the comparison between the different received signals can not be performed simultaneously (Sherman, 1984). New algorithms, which analyze the pulses sequentially during the whole passage, have to be developed to extract the object RCS. The algorithms will pay special attention to 1-2 cm targets, which are detectable at 1000 km by the Effelsberg radio telescope but not with TIRA. At L-band wavelengths the vast majority of these small debris objects is characterized by a RCS practically independent of the observation angle, a RCS-size relationship through Rayleigh for-

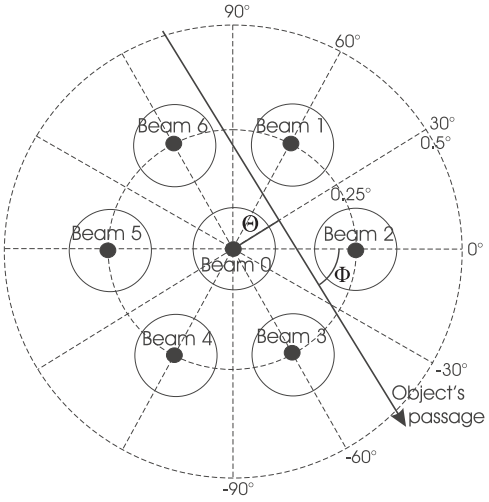

Figure 1. Footprint at the sky of the Effelsberg multi-beam system and an object's passage example .

mula (Eq. 1) and a poor SNR of the corresponding received signals.

$$RCS = \frac{9 \cdot \pi \cdot d^6}{4 \cdot \lambda^4} \tag{1}$$

The rest of this paper is organized as follows. After a brief description of the problem statement in section 2, section 3 explains the theoretical basics of the developed algorithms. The performance of the proposed algorithms is studied through Cramer-Rao Lower Bound, Monte-Carlo simulations and a couple of illustrative examples in section 4. Finally, some concluding remarks are reported in section 5.

2. PROBLEM STATEMENT

Taking the multi-beam system shown in Fig. 1 into account, the primary task of this work is the determination of the space debris RCS and the trajectory parameters of its passage through the overlapping volume between the beams of TIRA and the Effelsberg radio telescope by processing obtained multi-beam data. The main trajectory parameters are the passage offset (Θ), the passage direction (Φ), the passage inclination with respect to the projection plane (α), the time of closest approach to the line of sight (t_{CPA}), the velocity (v) and the range at CPA (R_{CPA}). These six parameters together will be sufficient to be able to characterize the passage unambiguously, if the two parallel paths with the same offset are distinguished by means of a different sign. To simplify the notation the six trajectory parameters are gathered into a vector parameter (ω), that means $\omega = [\Theta, \Phi, \alpha, t_{CPA}, v, R_{CPA}]$.

The received power signals by each horn can be calculated through the bi-static radar equation (Eq. 2), where index i symbolizes any signal or gain pattern of the Effelsberg 7-beam system and takes values between 0 and 6. P_r^i symolizes the received power, P_t the transmitted power, G the antenna gain pattern and R the ranges. L is the total losses and gathers the losses in the transmitter L_t, the atmospheric losses L_{at} and the losses in the receiver L_r (Eq. 3).

$$P_r^i = \frac{P_t \cdot \lambda^2 \cdot RCS \cdot G_{TIRA}(\omega) \cdot G_{EFFE}^i(\omega)}{(4\pi)^3 \cdot R_{EFFE}^2 \cdot R_{TIRA}^2 \cdot L} \tag{2}$$

$$L = L_t \cdot L_{at}^2 \cdot L_r \tag{3}$$

Actually, the received power will be also affected by the system noise, since both I and Q components will be corrupted by a zero-mean gaussian noise. The system noise power, that is, the variance of the noise σ^2, will be measured during the observation campaign. In the case of COBEAM-1/96, the NERCS (Noise Equivalent Radar Cross Section) added up to -68 dBsm at 1000 km. The actual received power Y^i will follow the statistic shown in Eq. 4.

$$Y^i = \left(\sqrt{P_r^i} + N_I^i\left(0, \frac{\sigma^2}{2}\right)\right)^2 + N_Q^i{}^2\left(0, \frac{\sigma^2}{2}\right) \tag{4}$$

In short, the problem lies in the estimation of the object RCS and its trajectory parameters ω according to available multi-beam data Y^i grouped into the vector $\underline{Y}$.

3. ALGORITHMS FOR MULTI-BEAM DATA ANALYSIS

3.1. Non-Statistical approaches

This class of algorithms summarizes all methods with an analytical character. For example, the passage direction could be calculated from corresponding time differences between the intensity maxima in a reference beam and the other six horns, if all beam patterns were assumed circular symmetric (actually, they are not). These algorithms require a very low computational effort, but offer an insufficient accuracy for noisy signals and actual beam patterns.

3.2. LSE: Least-Square Estimation

An important feature of the LSE methods is that no probabilistic assumptions have to be made about available data. Therefore in general these methods have no optimality properties (Kay, 1993). Data is firstly modelled according to Eq. 2 without taking the noisy components (Eq. 4) into account and subsequently, the unknown parameters (RCS and ω) are estimated by the minimization of the square error between modelled and actual data. The minimization process is implemented by an initial coarse grid search followed by an iterative search by the Nelder-Mead method.

3.2.1. LSE1: a first possibility of LSE

Under the assumption of a constant RCS during the whole passage, the quotient between any two received signals is equivalent to the quotient between the corresponding Effelsberg beam gain patterns. This relationship is shown in Eq. 5, where i and j symbolize any two different beams of the multi-beam system. The relationship is also true for all received pulses. Two matrices, the first one of quotients between received signals and the second one of quotients between Effelsberg beam gain patterns, are built by gathering all possible combinations between beams and all received pulses. The trajectory parameters w are estimated by the minimization of the square difference between both matrices. Weighting matrices have to be also applied in order to penalize noisier signal combinations. The RCS is estimated through a second least square method via Eq. 2, where the previously calculated trajectory parameters ω were already substituted. The sequential computation of the parameters is very interesting from the computational effort point of view.

$$\frac{Y^i}{Y^j} = \frac{G^i_{EFFE}(\omega)}{G^j_{EFFE}(\omega)} \tag{5}$$

3.2.2. LSE2: a second possibility of LSE

The computation of the quotients in LSE1 does not turn out to be statistically advisable, since the very noisy echoes degrade the corresponding quotients severely. An independent data analysis of each beam would render more accuracy. Therefore, in LSE2 the parameters are estimated by minimization of the square difference between actual data Y^i and modelled data P^i_r. Nevertheless, LSE2 has the weakness that both parameters RCS and ω have to be evaluated simultaneously.

3.3. MLE: Maximum Likelihood Estimation

Unlike the Least-Square techniques, the maximum likelihood estimations (MLE) take the noise and its statistics into account. The maximum likelihood estimates correspond to the values of the parameters that maximize the data likelihood function (Kay, 1993). In general, the MLE has the asymptotic properties of being unbiased and achieving the CRLB (Cramer-Rao Lower Bound). The maximization processes are also implemented by an initial coarse grid search followed by an iterative search by the Nelder-Mead method. In order to simplify the notation of Eq. 2, let G be the product of both antenna patterns and a the collection of all constant values during the passage. Eq. 6, 7 and 8 clarify the simplifications made in Eq. 2.

$$\underline{G}(\omega) = G_{TIRA}(\omega) \cdot G^i_{EFFE}(\omega) \quad \text{for} \quad i = 0 \dots 6 \tag{6}$$

$$a = \frac{P_s \cdot \lambda^2 \cdot RCS}{(4\pi)^3 \cdot R^2_{EFFE} \cdot R^2_{TIRA} \cdot L} \tag{7}$$

$$\underline{P_r} = a \cdot \underline{G}(\omega) \tag{8}$$

3.3.1. GMLE: MLE for Gaussian noise

For sufficient SNR, both orthogonal I and Q Gaussian noise components may be substituted by only one I Gaussian noise component (Eq. 9), since the Q noise component does not have a serious effect on amplitude data $\sqrt{\underline{Y}}$. This approximation is implemented by the GMLE algorithm.

$$\sqrt{\underline{Y}} = \sqrt{\underline{P_r}} + \underline{N_I}\left(0, \frac{\sigma^2}{2}\right) \tag{9}$$

Knowing the Gaussian PDF of the noise and taking Eq. 9 into account, the likelihood function of amplitude data $\sqrt{\underline{Y}}$ depending on the parameters a and ω may be described through Eq. 10, where n symbolizes the number of echoes.

$$LF\left(\sqrt{\underline{Y}}; a, \omega\right) = \left(\frac{1}{\sqrt{\pi} \cdot \sigma}\right)^{7 \cdot n} \cdot e^{-\frac{|\sqrt{\underline{Y}} - \sqrt{a \cdot \underline{G}(\omega)}|^2}{7 \cdot n \cdot \sigma^2}} \tag{10}$$

The estimation of the parameters will be performed by the maximization of the likelihood function (Eq. 10). The parameters can be estimated independently, since the differential equation can be solved in closed form. This reduces the necessary computational effort of the estimation. The trajectory parameters will be estimated by the values which maximize the absolute value of the cross-correlation between the vector of received signals and the corresponding normalized gain pattern vectors (Eq. 11). The estimation of a is performed with the estimated trajectory parameter through Eq. 12. The estimates of the parameters are symbolized by $\widehat{a}$ and $\widehat{\omega}$.

$$\widehat{\omega} = \max \left\{ \left| \underline{Y}^T \cdot \frac{\underline{G}(\omega)}{|\underline{G}(\omega)|} \right| \right\} \tag{11}$$

$$\widehat{a} = \frac{\underline{Y}^T \cdot \underline{G}(\widehat{\omega})}{|\underline{G}(\widehat{\omega})|^2} \tag{12}$$

3.3.2. RMLE: MLE for Ricean distributed data

Due to the two Gaussian noisy components of Eq. 4, the received amplitudes in the multi-beam system have a Ricean probability density (Rosebrock, 1999). The Ricean probability density is shown in Eq. 13, where I_o is the modified Bessel function of the first kind and order zero, and j symbolizes any of $7 \cdot n$ received echoes. The joint probability density of received amplitude vector $\sqrt{\underline{Y}}$ is the product of the individual probabilities because they are statistically

independent by assumption.

$$p\big(\sqrt{Y_j};a,\omega\big)= \sqrt{Y_j}\cdot e^{-\frac{Y_j+a\cdot G_j(\omega)}{2}}\cdot I_o\Big(\sqrt{Y_j\cdot a\cdot G_j(\omega)}\Big) \tag{13}$$

Thus, the RMLE method estimates the parameters by maximization of the log-likelihood function, that is shown in its simplified form in Eq. 14.

$$\begin{aligned}\ln\big(LF\big(\sqrt{\underline{Y}};a,\omega\big)\big) &= \sum_{j=1}^{7\cdot n}\ln\Big(I_o\Big(\sqrt{Y_j\cdot a\cdot G_j(\omega)}\Big)\\ &\quad -\frac{a}{2}\cdot\sum_{j=1}^{7\cdot n}G_j(\omega)\end{aligned} \tag{14}$$

Unfortunately an analytical calculation of the ML estimates from Eq. 14 is not possible, because the solution of the differential equation results in a difficult nonlinear constrained problem and no closed-form solution is available. Several approximations were also tested to simplify the solution process, but the results were not positive either:

- $ln(I_o(x)) \approx x$ leads to GMLE.
- $ln(I_o(x)) \approx x - \frac{1}{2}\cdot ln(2\cdot\pi\cdot x)$ is suitable at high SNR but diverges toward plus infinity at low SNR.
- $ln(I_o(x)) \approx \frac{x^2}{4} - \frac{x^4}{64}$ is suitable at low SNR but diverges toward minus infinity at high SNR.

For these reasons the estimation of all parameters has to be performed simultaneously by maximizing Eq. 14 iteratively.

4. PERFORMANCE OF PROPOSED ALGORITHMS

4.1. Cramer-Rao Lower Bounds

The fundamental limitation in an estimation problem is often assessed using the Cramer-Rao Lower Bound (CRLB), which is a lower bound on the estimation error variance for any unbiased estimator. The CRLB provides a benchmark against which we can compare the performance of any unbiased estimator, in this case, the accuracy of the proposed algorithms (Kay, 1993).

The determination of the CRLB consists mainly in taking the derivates of Eq. 14 with respect to the unknown parameters and subsequently the calculation of the expectation with respect to the actual data PDF. Mathematical expressions for the elements of the Fisher Information matrix $I(a)$ and $I(\omega_k)$ corresponding to the parameters a and ω_k are presented in Eq. 15 and Eq. 16 respectively, where the integral A_j (Eq. 17) could not be calculated in an explicit form and had to be computed numerically. I_1 symbolizes the modified Bessel function of the first kind and order one, whereas $G'_j(\omega)$ represents the first derivative of the antenna pattern with respect to the corresponding trajectory parameter ω_k.

$$I(a) = \sum_{j=1}^{7\cdot n} G_j(\omega)\cdot\big(2 + A_j - a^2\cdot G_j(\omega)\big) \tag{15}$$

$$\begin{aligned}I(\omega_k) &= a\sum_{j=1}^{7\cdot n}G'_j(\omega)\cdot A_j - a^2\sum_{j=1}^{7\cdot n}G_j(\omega)\cdot G'_j(\omega) +\\ &\quad +3a^2\Big(\sum_{j=1}^{7\cdot n}\sqrt{G_j(\omega)\cdot G'_j(\omega)}\Big)^2\end{aligned} \tag{16}$$

$$A_j = \int_0^\infty \frac{Y_j}{2}\cdot\frac{I_1^2\big(\sqrt{a\cdot G_j(\omega)\cdot Y^j}\big)}{I_0\big(\sqrt{a\cdot G_j(\omega)\cdot Y^j}\big)}\cdot e^{-\frac{Y_j+a\cdot G_j(\omega)}{2}}\cdot dY_j \tag{17}$$

The CRLBs for the estimation of the parameters are the inverse of the corresponding elements of the Fisher Information matrix.

4.2. Monte-Carlo Analysis

The performance of the algorithms explained in section 3 is analyzed through the root mean square estimation error for the object size, the passage offset and the passage direction. The estimation accuracy actually depends only on the SNR of the received signals. But on the other hand, the SNR is mainly depending on the object RCS and the attenuation by crossing the beam patterns (Eq. 2), since the SNR of received echoes corresponds to the RCS/NERCS relationship of the object attenuated by the gain patterns.

Firstly, the estimation accuracy depending on the object size is evaluated through Monte-Carlo simulations with 500 trials for passages through the overlapping volume with offset smaller than 0.25^o w. r. t. the Effelsberg antenna axis and an arbitrary passage direction. The root mean square object size estimation errors of the studied algorithms have been displayed in Fig. 2 for several object sizes. In the same way, Fig. 3 and 4 show the root mean square offset and direction estimation errors of the two MLE methods respectively.

The first clear result of the simulations is that the estimation accuracy of the Maximum Likelihood algorithms is substantially higher than in the Least-Squares approaches for the same computational effort due to its statistically better processing of the system noise. With regard to MLE algorithms GMLE proves to be a reasonable approach, but

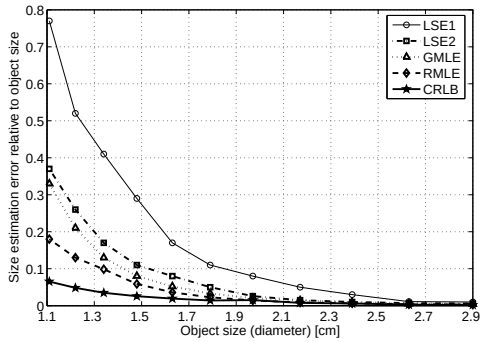

Figure 2. Size estimation error of the proposed algorithms as a function of the object size.

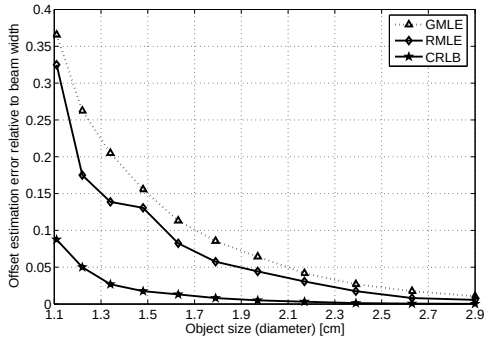

Figure 3. Passage offset estimation error of the MLE algorithms as a function of the object size.

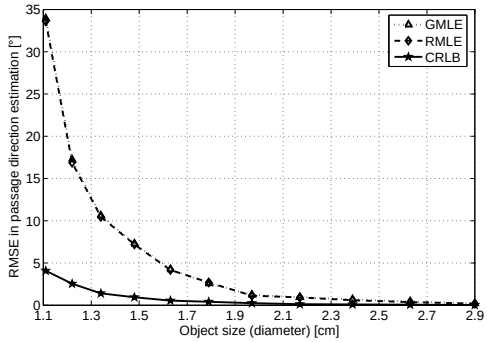

Figure 4. Passage direction estimation error of the MLE algorithms as a funtion of the object size.

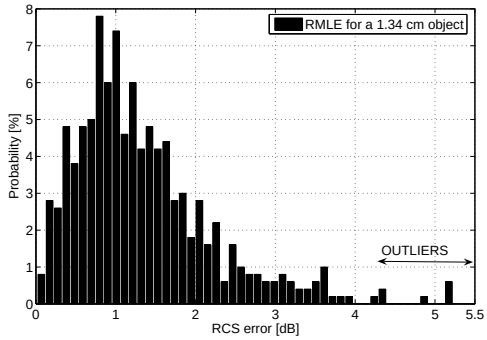

Figure 5. RCS error histogram of RMLE for a 1.34 cm object.

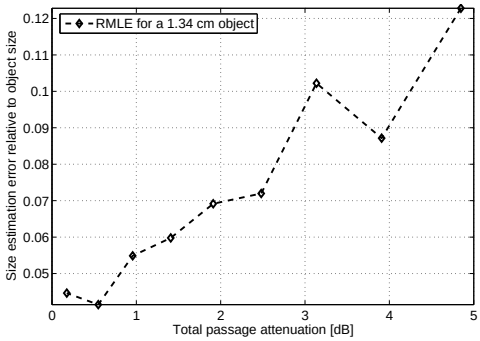

Figure 6. Size estimation error of RMLE as a function of the total passage attenuation for a 1.34 cm object.

RMLE estimations are still more accurately. In conclusion, the RMLE algorithm offers satisfactory qualities w. r. t. to accuracy and volume of applicability.

Anyway, the performance of RMLE does not achieve the CRLB, especially, for very small objects. This does not necessarily mean that a better estimation could be performed since the CRLB is far too optimistic at low SNR (Athley, 2002). It is known that nonlinear estimators usually exhibit a SNR threshold, below which the estimation error increases rapidly due to outliers. This effect is not captured by the CRLB, since it is a local bound that only considers small deviations from the true parameter value. At low SNR, noise may cause peaks in the likelihood function far away from the true peak to become the global maximum, yielding a large estimation error. This is then called an outlier, which will cause the MSE of the ML estimator to deviate from the CRLB. The RCS error histogram of RMLE simulation results for a 1.34 cm object is shown in Fig. 5, where some outliers can be clearly observed.

Actually, the SNR of the received echoes depends not only on the object size, but also on the attenuation caused by crossing the antenna patterns. This attenuation will be a function of the object trajectory. Intuitively, one can perform a better parameter estimation for passages crossing three beams than for outer passages (e.g. offsets larger than 0.2^o). This is illustrated in Fig. 6, where the object size estimation error depending on the total passage attenuation relative to the minimal attenuation passage is analyzed for a 1.34 cm object. Simulation results of Fig. 6 demonstrate that the parameters of the objects with lower attenuation during the passage can be more accurately estimated.

4.3. Two illustrative examples

In order to illustrate the satisfactory quality of RMLE, Fig. 7 provides an example of a 1.63 cm object with strong attenuation during the passage and

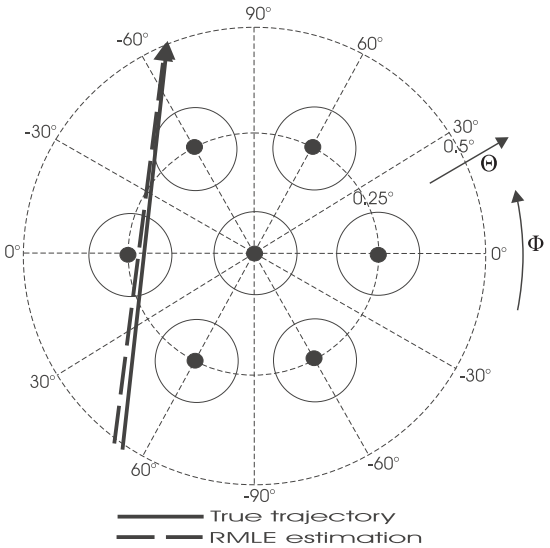

Figure 7. Estimation of a 1.63 cm object with strong attenuation during the passage.

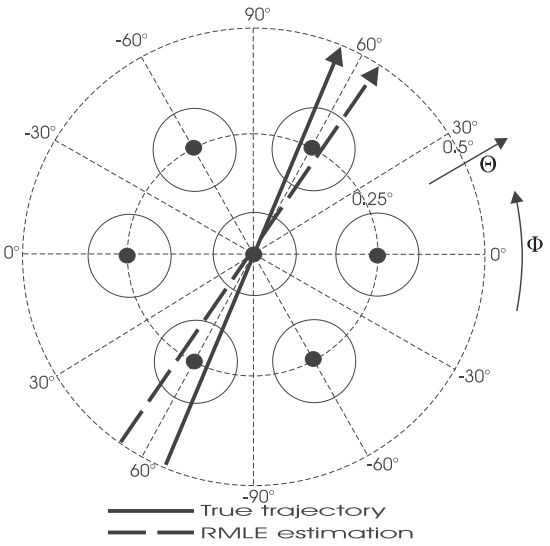

Figure 8. Estimation of a 1.22 cm object with weak attenuation during the passage.

Fig. 8 of a 1.22 cm object with lower attenuation. Fig. 8 is also an example of outliers, since the ambiguities of the antenna patterns could not be appropriately solved.

5. CONCLUDING REMARKS

Because of its satisfactory estimation accuracy and its large volume of applicability, RMLE is finally proposed as the suitable analysis algorithm for multi-beam data of the future TIRA-Effelsberg debris observation campaigns. RMLE will allow an accurate size estimation of objects in the 1-2 cm size. In order to reduce the computational effort of the iterative search processes in RMLE, initial estimations will be performed through GMLE.

It is known that, if an estimator achieving the CRLB exits, the MLE will achieve the CRLB too. Therefore, the performance of MLE might serve as an indicator, although not strictly a bound, of the ultimate estimation accuracy that can be achieved. Other estimation methods were also studied, but in our case their performance would be equivalent to MLE: Expectation-Maximization (EM), an iterative implementation of MLE for real-time estimations, and Bayesian techniques, in which the parameter of interest is considered as a random variable whose particular realization has to be estimated. For Bayesian estimations a priori probabilities of the parameters are needed, but in our case these distributions are not available. If uniformly distributed parameters were assumed, the Maximum A Posteriori (MAP) estimation would be equivalent to MLE proposed in this work.

ACKNOWLEDGMENTS

The author is very thankful to his colleagues of FGAN-FHR's Division Radar Techniques for Space Reconnaissance (RWA) for their important collaboration. This work was performed under ESA/ESOC contract no. 17820/03/D/HK(SC).

REFERENCES

Leushacke L., Mehrholz D., Jehn R., *First FGAN/MPIfR cooperative debris observation campaign: experiment outline and first results*, Proceeding of the second European Conference on Space Debris, ESA-ESOC Darmstadt, Germany, 1997, 45-50.

Sherman S. M., *Monopulse Principles and Techniques*, Artech Hause, Dedham 1984.

Kay S. M., *Fundamentals of Statistical Signal Processing. Vol. 1 Estimation Theory*, Prentice Hall PTR, New Jersey 1993.

Rosebrock J., Leushacke L., Mehrholz D., *Cooperative Debris Tracking and Development of Algorithms for Mid-Size Debris Detection with Radar*, Final Report of ESA/ESOC Study Contracts No. 12248/97/D/IM and No. 12247/97/D/IM, Wachtberg 1999.

Athley F., *Threshold Region Performance of Maximum Likelihood DOA Estimation for a Single Source*, In Proc. 10^{th} ASAP Workshop, MIT Lincoln Lab., Lexington, MA, USA, 2002.